Reorientational dynamics of molecules in liquid methane: A molecular dynamics simulation study

Article *in* Journal of Molecular Liquids · November 2020

DOI: 10.1016/j.molliq.2020.114727

3 authors:

Monika Madhavi
University of Colombo
11 PUBLICATIONS **20** CITATIONS
SEE PROFILE

Samantha Weerasinghe
University of Colombo
71 PUBLICATIONS **1,501** CITATIONS
SEE PROFILE

Konstantin Momot
Queensland University of Technology
74 PUBLICATIONS **825** CITATIONS
SEE PROFILE

Journal of Molecular Liquids xxx (xxxx) xxx

Contents lists available at ScienceDirect

Journal of Molecular Liquids

journal homepage: www.elsevier.com/locate/molliq

Reorientational dynamics of molecules in liquid methane: A molecular dynamics simulation study

W.A. Monika Madhavi [a,b], Samantha Weerasinghe [c], Konstantin I. Momot [a,*]

[a] School of Chemistry and Physics, Queensland University of Technology (QUT), GPO Box 2434, Brisbane, QLD 4001, Australia
[b] Department of Physics, University of Colombo, Colombo 03, Sri Lanka
[c] Department of Chemistry, University of Colombo, Colombo 03, Sri Lanka

ARTICLE INFO

Article history:
Received 12 June 2020
Received in revised form 25 September 2020
Accepted 5 November 2020
Available online xxxx

Keywords:
Molecular dynamics in liquids
Rotational diffusion
Reorientational motion of molecules

ABSTRACT

Rotational motion of molecules in liquids plays an important role in determining the liquids' Nuclear Magnetic Resonance (NMR) spin-relaxation properties. The traditional theory of NMR spin relaxation assumes that the reorientational dynamics of molecules in liquids can be described by a continuous-time rotational-diffusion random walk with a single rotational-diffusion coefficient. However, recent experimental and theoretical studies have demonstrated that the simple rotational-diffusion model does not fully capture the rotational dynamics of molecules in liquids: for example, the reorientation of molecules in liquid water occurs through a combination of continuous-time rotational diffusion and discrete, large angular jumps resulting from collective rearrangements of the hydrogen-bond network of water.

In order to obtain further insights into the origin of large angular jumps in the rotational motion of liquid water, we studied the rotational dynamics of methane - an apolar, non-hydrogen-bonding liquid with a spherically symmetric molecule. The reorientational propagator and the ensemble-averaged Legendre polynomial reorientational functions of liquid methane were analysed using molecular dynamics simulations. On the femtosecond timescale, the reorientational motion of methane molecules was found to be characterised by free-rotation gas-like Gaussian decay of the reorientational Legendre polynomials, a result consistent with the available experimental data for liquid methane. On the long timescale (picoseconds) the decay of the reorientational Legendre polynomials was exponential, suggestive of a Debye-like continuous-time rotational diffusion behaviour. However, the ratios of the exponential time constants for different orders of the Legendre polynomials failed to match the rotational-diffusion model. We discuss the implications of these findings for the understanding of rotational motion of molecules in hydrogen-bonding and non-hydrogen-bonding liquids.

1. Introduction

Rotational dynamics of molecules in liquids is determined by microscopic intermolecular interactions. In turn, rotational molecular dynamics determines many macroscopic properties of the liquid, making it an important component of the link between the molecular and the macroscopic scale. Understanding of the reorientational behaviour of molecules in liquids is therefore important not only from the point of view of molecular physics, but also in many practical contexts. Experimentally, information about the rotational dynamics of molecules in liquids can be obtained from techniques such as infrared and Raman spectroscopy [1–4], NMR spin relaxation [5] and neutron scattering [6–9]. Interpretation of these experimental data requires the use of the appropriate theoretical model that describes how molecular reorientation occurs.

The majority of NMR spin-relaxation literature treats molecular reorientation in liquids using the Debye model, which describes molecular reorientation as a rotational random walk on the surface of a sphere [10,11]. The solution of the respective diffusion equation is the rotational diffusion propagator, which can be conveniently expressed as an expansion in terms of spherical harmonics. An extension of the Debye model to asymmetric molecules was given by Perrin [12]. These models are particularly suitable for describing the reorientational motion of large molecules in a homogeneous liquid made up of much smaller molecules.

However, the applicability of the Debye rotational-diffusion model is seriously questioned in the case of single-component molecular liquids. This is particularly apparent in liquid water, which has a strong hydrogen-bonding network and therefore represents an extreme example of a "strongly-interacting" molecular liquid. The shortcomings of the Debye model in liquid water have been postulated theoretically over 50 years ago [13] and definitively demonstrated in the early 2000's [14–16]. Molecular dynamics (MD) simulations, performed both by

* Corresponding author.
E-mail address: k.momot@qut.edu.au (K.I. Momot).

https://doi.org/10.1016/j.molliq.2020.114727
0167-7322/

Table of symbols

Δ_S	angular part of the 3D Laplacian operator
D	Debye rotational diffusion coefficient
Ψ	rotational diffusion propagator
$\Upsilon_{l,m}$	spherical harmonics
$\tau_l = 1/Dl(l+1)$	Debye rotational time constants
Ω_0, Ω	orientation of a vector fixed relative to the rotating molecule at times 0 and t, respectively
k	Boltzmann constant
T	temperature
η	dynamic viscosity of the liquid
r	effective hydrodynamic radius of the molecule
P_l	l-th-rank Legendre polynomial
α	angular displacement
$F = kT/I$	Free-rotation coefficient
I	moment of inertia of the molecule
r	is the distance between a pair of particles
$p(r, r+dr)$	average number of C–C atom pairs within the spherical shell $r \ldots r+dr$
N_{pairs}	number of unique pairs of atoms in the system
V	total volume of the system
A, B, C	Amplitudes of individual Gaussian or exponential decay components of correlation functions
D_{fit}, D_{1fit}, D_{2fit}	Apparent Debye rotational-diffusion coefficients
F_{fit}	Apparent free-rotation coefficient
$a = F\,l(l+1)/2$	Apparent Gaussian time constant

other researchers [14,15,17–19] and by us [20], have shown that the rotational dynamics of water molecules in liquid water fail to follow the Debye form of the rotational-diffusion propagator characterised by a single rotational-diffusion coefficient. Rather, rotational reorientation of water molecules in the long-time regime (0.5–100 ps) was found to occur *via* a superposition of two mechanisms: "true" continuous-time rotational diffusion and large-angle "instantaneous" jumps associated with collective rearrangements of the hydrogen-bonding network. The latter mechanism is distinct from the Debye-type rotational diffusion: when an existing hydrogen bond between two water molecules is broken and a new bond is formed with another neighbouring water molecule, a water molecule can be found to be rotating by an anomalously large angle within a very short time interval. Therefore, both diffusion and hydrogen bonding play a crucial role in the reorientational dynamics of water molecules [21,22]. The presence of the two mechanisms of molecular reorientation also distorts the ratios of the rotational correlation times associated with different orders of reorientational Legendre polynomials. In our own MD study of liquid water, we observed that the reciprocal time constants of Legendre polynomial functions of orders 1–4 ($1/\tau_1$, $1/\tau_2$, $1/\tau_3$, $1/\tau_4$) exhibited strongly non-ideal ratios, 1 : 2.0 : 3.0 : 3.8, that significantly deviated from the Debye's theoretical ratios, 1 : 3 : 6 : 10 [20]. This deviation can be used as a measure of how "far" the liquid is from the pure rotational-diffusion regime.

The opposite extreme is the case of apolar or low-polarity liquids such as liquid nitrogen or hydrogen sulphide. In these cases the Debye rotational-diffusion model is also known to fail, albeit for reasons opposite to those seen in water: intermolecular interaction in these liquids can be too weak for them to be in the overdamped regime of Langevin dynamics that gives rise to pure Brownian motion. Empirical rotational autocorrelation functions for such liquids have been obtained from Raman and infrared data [1]. These functions strongly deviated from the Debye rotational-diffusion model in that the Legendre polynomial correlation functions did not exhibit an exponential decay. Gordon [23] has theoretically interpreted these results for linear molecules in simple liquids using the model of free rotation interrupted by instantaneous collisions. During a collision, the angular momentum of the molecule is changed but the orientation of the molecule is considered to remain unchanged. Two limiting cases of Gordons' extended model have been identified as m-diffusion and j-diffusion. In the m-diffusion limit, the direction of the angular momentum vector is randomised at every collision but the magnitude remains unchanged. In the j-diffusion limit, both the direction and the magnitude of the angular momentum vector are randomised according to the Boltzmann distribution. The free-rotation model gives the short-time limiting case of Gordons' model, while the Debye rotational-diffusion model gives its long-time limiting case. The model was later developed by McClung [24] to describe the rotational dynamics of spherical-top molecules.

The key aim of the present study was to use all-atom Molecular Dynamics simulations in order to obtain a detailed understanding of the rotational dynamics of molecules in "weakly-interacting" liquids free of hydrogen bonding. Previously we have used hydrogen sulphide as a test molecule to explore the applicability of the Debye model to liquids that are weakly polar but free of hydrogen-bonding networks [25]. In the present work, we extend this approach to methane. Besides being an apolar molecule that does not form hydrogen bonds, methane is also spherically symmetric. We therefore used this molecule as a test case to examine the performance of the Debye model in a non-hydrogen bond-forming liquid consisting of spherical-top molecules [26,27]. We performed molecular dynamics simulations of liquid methane and analysed the rotational dynamics of methane molecules and their compatibility with the Debye model. We tested the capability of three sets of force field parameters that have been used previously for MD simulations of methane, to accurately reproduce experimentally obtained rotational correlation functions, and used the best-performing set of force field parameters to study the rotational dynamics of methane in detail. Using the resulting MD trajectories, we quantified the rotational correlation functions and the reorientational propagator of methane within a time range from femtoseconds to picoseconds. The results demonstrate that, despite the spherical symmetry and the absence of a hydrogen-bonding network, the Debye model still fails to provide a comprehensive description of molecular reorientation of methane. In the short-time regime (tens to hundreds of femtoseconds) the reorientation of methane molecules in our simulations was adequately described by the gas-like free-rotation model [6], which is characterised by Gaussian decay of the rotational Legendre polynomials and consistent with the available experimental data [3,4,6,28]. In the long-time (picosecond) regime, we have observed an unexpected exponential decay of the Legendre polynomials suggestive of Debye-like rotational diffusion. However, the ratio of the time constants of the polynomials of orders 1 and 2 was close to 1, *i.e.* very far from the ideal ratio of 1:3. We discuss these findings in the following sections.

2. Theory

2.1. Debye's rotational diffusion model

Rotational diffusion of molecules in a liquids can be modelled using the angular part of the three-dimensional diffusion equation:

$$\frac{\partial \Psi}{\partial t} = D\Delta_S \Psi \tag{1}$$

where Δ_S is the angular part of the 3D Laplacian operator; D is the rotational diffusion coefficient; and Ψ is the rotational diffusion propagator that represents the solution of Eq. (1) and describes the conditional probability density of molecular orientation at time t.

The solution of the rotational diffusion equation for spherical molecules was given by Debye [10]:

$$\Psi(\Omega,\Omega_0,t)=\sum_{l=0}^{\infty}\sum_{m=-l}^{l}\Upsilon^{*}_{l,m}(\Omega_0)\Upsilon_{l,m}(\Omega)e^{-\frac{t}{\tau_l}} \tag{2}$$

where $\Upsilon_{l,m}$ are the spherical harmonics; the rotational time constants τ_l are related to the rotational diffusion coefficient: $\frac{1}{\tau_l}=Dl(l+1)$; Ω is the orientation of a vector fixed relative to the rotating molecule at a given time t; and Ω_0 is the orientation of the same vector at $t=0$. The rotational diffusion coefficient D is commonly given by the Stokes-Einstein relationship:

$$D=\frac{kT}{8\pi r^3\eta} \tag{3}$$

where D is measured in rad^2/s, k is the Boltzmann constant, T is the temperature, η is the dynamic viscosity of the liquid and r is the effective hydrodynamic radius of the molecule.

As an alternative to the diffusion propagator, rotational correlation functions based on Legendre polynomials are often used. Consider a unit-length vector fixed relative to a rotating molecule. The cosine of the angular displacement (α) of that vector at a given time can be calculated by taking the scalar product between the corresponding vector at the initial time $t_0=0$ and the current time t. Then the ensemble-averaged orientational correlation functions $<P_l(\cos\alpha,t)>$ (where P_l is the l-th-rank Legendre polynomial) describe the reorientational dynamics of the molecules within the liquid. For $l=1$, the function $<P_1>$ is simply the ensemble-averaged cosine of the angular displacement, $<\cos(\alpha),t)>$. When the rotational diffusion propagator is given by Eq. (2), the time dependence of the ensemble-averaged Legendre polynomial functions takes the form of an exponential decay:

$$\langle P_l(\cos\alpha,t)\rangle=e^{-Dl(l+1)t} \tag{4}$$

where the rotational diffusion coefficient D can be approximated by Eq. (3).

2.2. Gordon's free-rotation model

Experimental data shows that on time scales ~0.1 ps or shorter molecular reorientation in liquid methane is gas-like rather than liquid-like [1,3,29]. Methane is not unique in this respect: gas-like rotational characteristics have been observed in a number of liquids. For example, intensity distributions consistent with free molecular rotation have been observed in the Raman spectra of liquid oxygen and nitrogen, as well as methane [29]. The basic assumption of the Debye model, that molecular displacement within a time step Δt is represented by a small angular step $\Delta\theta=\sqrt{4D\Delta t}$, is not valid for the rotation of molecules in gases, because in a gas the molecules are able to reorient freely between collisions. Rotational motion of molecules in gases is usually modelled using the free-rotation model. The ensemble-averaged Legendre-polynomial functions in the case of gas-like rotation take the following form [3,6]:

$$\langle P_l(\cos\alpha,t)\rangle=\frac{1}{2l+1}\left(1+2\sum_{\xi=1}^{l}\left(1-\xi^2t^2D_f\right)e^{-\frac{\xi^2t^2F}{2}}\right) \tag{5}$$

where $F=kT/I$ is the free-rotation coefficient; k is the Boltzmann constant, T is the temperature and I is the moment of inertia of the molecule. It is worth noting that, despite both appearing in exponential attenuation functions, the rotational diffusion coefficient D and the free-rotation coefficient F have different physical meanings: these are reflected in their different physical units, s^{-1} and s^{-2}, respectively.

3. Methods

3.1. Selection of force field parameters for MD simulations

Prior to the production MD simulations, a set of MD force field parameters that is capable of reproducing the key experimental results concerning liquid methane was identified. Three all-atom models of methane, which have been previously used for liquid phase simulations [30–34], were tested for their capability to reproduce the experimentally obtained density [36], C–C radial distribution function [37,38], and rotational correlation functions [1,6] of methane. The molecular mechanics force fields tested were constructed by substituting the values of the parameters in the potential energy function used by the CHARMM force field [30] (Eq. (6)). The values of the three sets of parameters of methane force fields I, II and III are given in Table 1, and the detailed methodology of force field validation is given in Supplementary Material sections S2 - S5. The density values, C–C radial distribution functions and rotational Legendre polynomial functions calculated from the MD trajectories were compared to the corresponding experimental data in order to select the best set of force field parameters.

$$\begin{aligned}U=&\sum_{bonds}k_b(b-b_0)^2+\sum_{angles}k_\theta(\theta-\theta_0)^2+\sum_{dihedrals}k_\chi(1-\cos(n\chi-\delta))\\&+\sum_{impropers}k_{imp}(\varphi-\varphi_0)^2+\sum_{Urey-Bradley}k_{UB}(S-S_0)^2\\&+\sum_{nonbond}\epsilon\left[\left(\frac{R_{min_{ij}}}{r_{ij}}\right)^{12}-2\left(\frac{R_{min_{ij}}}{r_{ij}}\right)^{6}\right]+\frac{q_iq_j}{\epsilon_1r_{ij}}\end{aligned} \tag{6}$$

Of the three parameter sets tested, set III was found to best match each of the experimentally observed characteristics examined (density, C–C radial distribution function and rotational correlation functions). This parameter set was therefore used in all subsequent MD simulations.

3.2. Calculation of the rotational correlation functions

Production-run simulations of the rotational dynamics of liquid methane were performed in the NPT ensemble at $T=98$ K, $p=1$ atm using the following steps:

(1) The methane box containing 2000 molecules was energy-minimised for 10,000 steps.
(2) The energy-minimised system was heated from 0 K to the target temperature in the NVT ensemble for 40 ps with a step size of 2 fs. (The 2 fs time step was used only for equilibration.)
(3) The system was further equilibrated in the NPT ensemble at the target temperature, $p=1$ atm for 120 ps in steps of 2 fs.
(4) The output of step (3) was used as the initial configuration of a MD production run with the length 100 ps and a step size of 1 fs. The output coordinates were saved every 1 fs.

Table 1
Parameters of the three force fields tested in the present study.

Parameter	Atom(s)	Force field		
		I [31,35]	II [32]	III [30,33,34]
$\frac{\epsilon_{ab}}{k_B}$ (K)	C–C	33.212	46.8	10.07
	H–H	15.097	6.30	2.77
	C–H		17.17	
σ_{ab} (Å)	C–C	3.50	3.45	4.12
	H–H	2.50	2.67	2.64
	C–H		3.06	
q (e)	C	−0.24	−0.572	−0.360
	H	+0.06	+0.143	+0.090
b_0 (Å)	C–H	1.09	1.087	1.1110
θ_0 (deg)	H–C–H	107.8	107.8	108.40
k_b (KJ mol^{-1} Å^{-2})	C–H	2845.12	2845.12	2694.5
k_θ (KJ mol^{-1} rad^{-2})	H–C–H	276.14	276.14	297.06
k_{UB} (kcal mol^{-1} rad^{-2})	H–C–H			5.40
	H–C–C			22.53
S_0 (Å)	H–C–H			1.8020
	H–C–C			2.1790

For the tracking of the rotational dynamics, the unit-length orientation vector of a C–H bond was output at a time interval of 1 fs for each of the 2000 methane molecules in the simulation box. The cosine of the angular displacement (α) of the C–H bond vector at each time step was calculated by taking the scalar product of the orientation vector of the corresponding C–H bond with the orientation vector of the same bond at the initial time ($t_0 = 0$). The orientational correlation functions $\langle P_l(\cos(\alpha)),t\rangle$ were then calculated, where P_l is the l-th rank Legendre polynomial ($l = 1$–4).

All the MD simulations were performed using NAMD 2.12 software. A Langevin thermostat with the damping coefficient of 1 ps^{-1} was used to control the temperature, and a Langevin piston with a piston period of 100 fs and decay period of 50 fs was used to control the pressure. Electrostatic interactions were calculated using the PME method with the cut-off distance of 10 Å and periodic boundary conditions were applied in all directions.

3.3. Least-squares fitting of rotational correlation functions

The trajectory of the production-run MD simulation of methane performed at $T = 98$ K, $p = 1$ atm with parameter set III (see Table 1) was used to investigate the rotational dynamics of methane molecules in liquid. The trajectory (100 ps long) was divided into 50 sub-trajectories, each of the length 2 ps. For each sub-trajectory, Legendre polynomial functions of the angular displacement of a single C–H vector, $P_l(\cos(\alpha_m(t_k)))$, were sampled for each molecule m at time points t_k (in steps of 1 fs) for $l = 1$–4. The ensemble-averaged Legendre polynomial functions of the orders $l = 1$–4 were then calculated by averaging the corresponding values of $P_l(\cos(\alpha_m(t_k)))$ over the 2000 molecules. The Legendre polynomial functions were then again averaged over the 50 sub-trajectories.

For each value of l, the values of $<P_l(\cos(\alpha),t_k)>$ were converted to the log scale and the quantity $\ln(<P_l(\cos(\alpha),t_k)>)$ were plotted against t_k. By visually examining the plot, two regions were identified for each value of l: a "Gaussian" region (quadratic decay of the semilog plot) and an "exponential" region (linear decay in the semilog plot). The Legendre polynomials P_l were then individually least-squares fitted in the following ways:

(1) The "exponential" regions for $l = 1$ and 2 were fitted in the semilog coordinates ($\ln<P_l>$ *vs* t) using a linearised fit model with the equation

$$f_d(t) = A - D_{fit}\, l(l+1)t \tag{7}$$

(2) The "exponential" regions for $l = 1$ and 2 were fitted in the original coordinates ($<P_l>$ *vs* t) using a nonlinear fit model $A \cdot exp[-D_{fit} l(l+1)t]$;

(3) The "Gaussian" regions were fitted in the semilog-time-squared coordinates ($\ln<P_l>$ *vs* t^2) using a linearised fit model with the equation

$$f_g(t) = A - at^2 \tag{8}$$

(4) The "Gaussian" regions were fitted in the original coordinates ($<P_l>$ *vs* t) using a nonlinear fit model $A \cdot exp[-at^2]$;

5) The entire curve $<P_l>$ *vs* t was fitted in the original coordinates using the nonlinear fit model with two distinct exponential components and a Gaussian component:

$$f(t) = A\exp(-a\,t^2) + B\exp(-D_{1fit}\,t) + C\exp(-D_{2fit}\,t) \tag{9}$$

The objective of least-squares fitting the Legendre polynomial curves using Eq. (9) was to test an analytic representation of the overall shape of the Legendre polynomial decay functions rather than obtain the quantitative values of the fitted parameters. The origin of the model given by Eq. (9) is discussed in the Discussion section (Subsection 5.5). In the Gaussian fitting (steps 3 and 4), in ideal case the fitted value of the parameter a equals $F\,l(l+1)/2$, where $F = kT/I$ is the Gordon model's free-rotation coefficient in units ps^{-2}. The apparent value of F was calculated separately for each value of $l = 1$–4. The difference between the parameter values obtained from linearised and nonlinear fits was used as a measure of the true uncertainty of the respective time constants. For $l = 3$ and 4, the fits of the "exponential" regions were considered unreliable because of the vanishingly low amplitude of the Legendre curves in the respective regions.

3.4. Comparison of NPT and NVE ensembles

In order to ensure that the MD simulation results were not affected by the temperature and pressure controls used in the NPT ensemble simulations, a 100 ps long test MD run was performed at 98 K without temperature or pressure controls (NVE ensemble) using parameter set III. The Legendre polynomial curves P_l ($l = 1$–4) were calculated from this NVE-simulated trajectory in the same way as described in Sections 3.2 and 3.3. The least-squares fitting procedure described in Section 3.3 was repeated for ensemble-averaged Legendre polynomial functions P_1 - P_4 obtained from the NVE simulations.

3.5. Least-squares fitting of the rotational diffusion propagator

Liquid methane is isotropic and the methane molecule has a T_d symmetry corresponding to spherically symmetric rotational-diffusion and inertia tensors. Therefore, in the Debye-like reorientational regime (which is identified in Sections 4 and 5) the reorientational motion of methane molecules can be described, without loss of generality, by a uniangular rotational-diffusion propagator $\Psi'(\alpha,t)$ that depends only on the absolute angular displacement, α [20]. The uniangular rotational-diffusion propagator $\Psi'(\alpha,t)$ can be obtained by integrating the three-dimensional rotational-diffusion propagator given by Eq. (2) with respect to the azimuthal angle ϕ. As the value of α at the initial time is zero by definition, the uniangular propagator contains a zero contribution from the spherical harmonics of non-zero orders ($m \neq 0$). The resulting uniangular propagator takes the form [20]

$$\Psi'(\alpha,t) = 2\pi \sum_{l=0}^{\infty} \Upsilon^*_{l,0}(0)\Upsilon_{l,0}(\alpha)e^{-\frac{t}{\tau_l}} \tag{10}$$

For each 2-ps sub-trajectory (see above), the orientations of a C–H vector in each of the 2000 methane molecules were sampled every1 f. from the MD simulation performed at $T = 98$ K, $p = 1$ atm. The angular displacements of the intramolecular C–H vectors were calculated for each time frame (k), each molecule (m) as

$$\alpha_m(t_k) = \arccos[\mathbf{n}_m(t_0)\cdot\mathbf{n}_m(t_k)] \tag{11}$$

where $\mathbf{n}_m(t_i)$ is the unit C–H vector of m-th molecule at i-th time. The distribution of α at time t_k was then obtained by grouping the values of $\alpha_m(t_k)$ ($m = 1\ldots2000$) into 50 equally sized bins covering the angular range from 0 to π. Each distribution was normalised so that its total area equalled 1. Then the full uniangular rotational diffusion propagator was constructed by taking the average of the 50 probability distributions calculated from each sub-trajectory.

As the first step of the least-squares fitting process, slices of the uniangular rotational diffusion propagator $\Psi'(\alpha,t)$ in the temporal dimension were individually least-squares fitted with the Debye diffusion propagator given by Eq. (10) truncated at $l_{max} = 50$ using the Levenberg −Marquardt method. The Mathematica "*NonlinearModelFit*" function was used for this purpose, and the fit was considered converged when the relative change in the sum of the squares of the residuals between iterative steps fell below the specified precision goal (10^{-8}). The number of the diffusion coefficients in the Debye model was then increased to two, and the slices of $\Psi'(\alpha,t)$ in the temporal dimension were again

least-squares fitted. The quality of the fit was evaluated by visually examining the distribution of fit residuals.

Fitting of the uniangular rotational-diffusion propagator simultaneously in the angular and temporal dimensions was started by including only the data points corresponding to long times ($1\ ps < t < 2\ ps$) in the fitting data set. Then the range of data was gradually increased by including data points corresponding to shorter times in the fitting data set, and the fitting was repeated while the distribution of the fit residuals was continuously examined. This approach is similar to that we used for fitting the rotational-diffusion propagator of water molecules in our earlier work [20]. When the fit residuals started to exhibit systematic deviations, the fitting process was terminated and the last range of the data set was considered to be the Debye-model range.

4. Results

4.1. Fitting of the ensemble-averaged Legendre polynomial functions

The reorientational Legendre polynomial decay curves of the orders $l = 1$–4 obtained from the NPT production run, as well as the respective least-squares fits, are shown in Fig. 1. The long-t "exponential" (Debye-like) regions of these curves could only be successfully fitted for $l = 1$ and 2; the results (based on the nonlinear exponential fits) are presented in Table 2. The ratios between the values of τ_l^{-1} for the orders $l = 1$ and 2 were 1: 1.2, which is a very significant deviation from the ideal ratio of 1: 3.

The short-t "Gaussian" (free gas-like rotation) regions were able to be successfully fitted for all four curves $l = 1$–4. The resulting parameters, based on the nonlinear Gaussian fits, are given in Table 3. The ratios between the quadratic coefficients (a) of the orders 1–4 were 1: 3.0: 6.1: 10.2, while the value of the free-rotation coefficient F was approximately constant for $l = 1$–4 (see Table 3: columns 3–6).

Table 2
Reorientational parameters extracted by least-squares fitting of the Debye-like (exponential) regime of the ensemble-averaged Legendre polynomial functions of NPT and NVE simulations.

l	Range (ps)	NPT simulation		NVE simulation	
		$\tau_l^{-1} = Dl(l+1)$ (ps^{-1})	Ratio	$\tau_l^{-1} = Dl(l+1)$ (ps^{-1})	Ratio
1	0.35–2	3.422 ± 0.004	1	3.396 ± 0.002	1
2	0.3–2	4.09 ± 0.02	1.2	4.42 ± 0.02	1.3

Table 3
Reorientational parameters extracted by least-squares fitting of the Gaussian (short-time) regime of the ensemble-averaged Legendre polynomial functions of NPT and NVE simulations. For comparison, the value of F calculated directly from methane's moment of inertia is 25.32 ps^{-2}.

l	Range (ps)	NPT simulation		NVE simulation	
		a (ps^{-2})	F (ps^{-2})	a (ps^{-2})	F (ps^{-2})
1	0–0.09	22.83 ± 0.06	22.83 ± 0.06	22.89 ± 0.06	22.89 ± 0.06
2	0–0.075	69.8 ± 0.3	23.3 ± 0.1	70.1 ± 0.3	23.4 ± 0.1
3	0–0.07	141.3 ± 0.6	23.6 ± 0.1	141.8 ± 0.6	23.6 ± 0.1
4	0–0.06	238.7 ± 1.5	23.9 ± 0.2	239.4 ± 1.5	23.9 ± 0.2

4.2. Comparison with the results of NVE simulation

According to the time constants reported in Tables 2 and 3 that were determined from the trajectories obtained from the NVE simulation, the

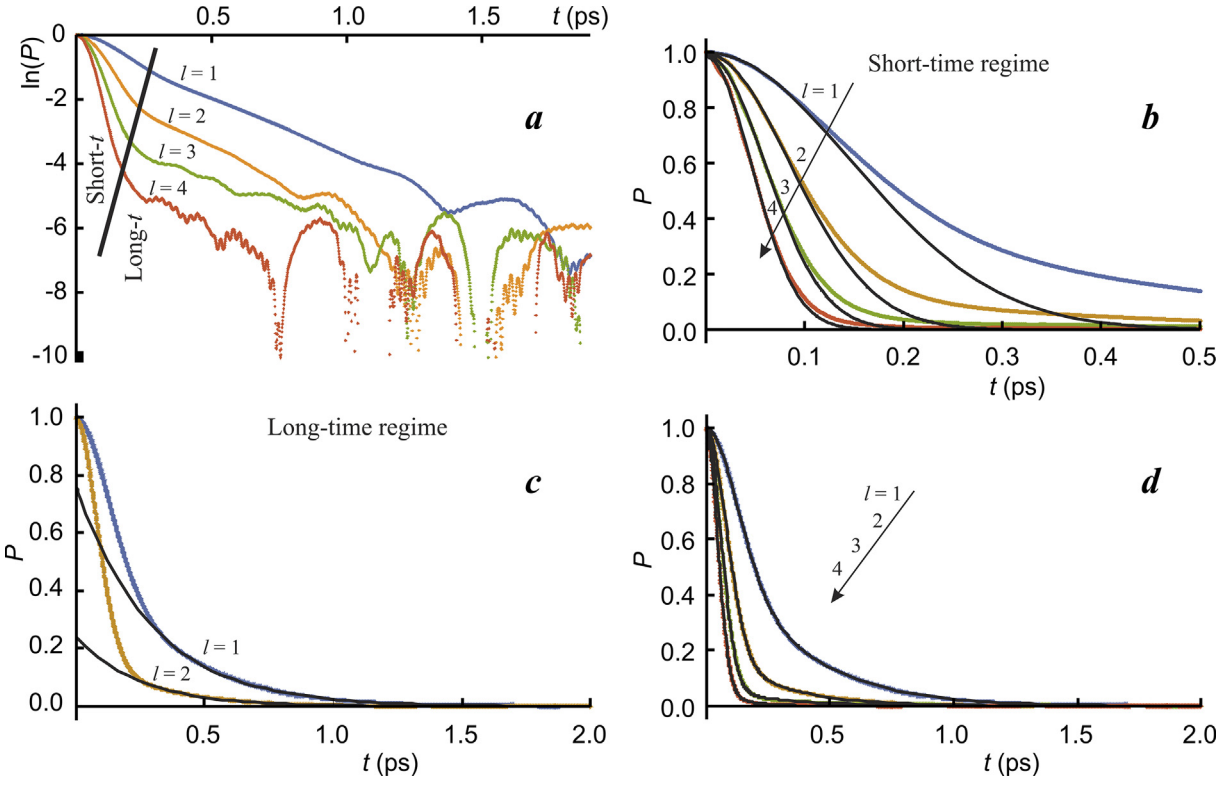

Fig. 1. The decays of reorientational Legendre polynomials of the orders l = 1–4 obtained from the NPT ensemble and their least-squares fits: (a) The plot in semilog coordinates enables identification of the free rotation-like ("Gaussian") regime and the Debye-like ("exponential") regime. The slanted solid line shows the approximate boundary between the two regimes. The least-squares fitting was performed in the original coordinates, <P > *vs* t: (b) Non-linear least-squares fits of the initial part of the decays ("Gaussian" regime) used to obtain the parameters shown in Table 3; (c) Non-linear least-squares fits of the tails of the decays ("exponential" regime) used to obtain the parameters shown in Table 2. This regime was fitted only for the curves l = 1 and 2 due to the preponderance of numerical artifacts in the higher-order polynomials; (d) Whole-curve fits performed using Eq. (9) for l = 1 and 2 and the same equation but without the third term for l = 3 and 4.

relative differences of τ_1^{-1} and τ_2^{-1} from the NPT values are −0.8% and + 8% respectively. The relative differences from the NPT values of the constants a_l (l = 1–4) were + 0.3%, +0.4%, +0.5% and + 0.3%. With the exception of τ_2^{-1}, the differences between the NPT and NVE values were considered insignificant. The difference between the two values of τ_2^{-1} could be considered significant compared to the standard error of the least-squares fitting procedure. However, this difference was negligible compared to the difference between the observed value of τ_2^{-1} and that expected from the Debye model (ideal $\tau_2^{-1} = 3\tau_1^{-1}$). Therefore, the NPT ensemble was deemed suitable for the simulation.

4.3. Reorientational propagator

Fig. 2 shows the uniangular reorientational propagator of a C–H vector of methane molecules calculated from the MD simulation trajectory at T = 98 K, p = 1 atm. This propagator is analogous to the rotational-diffusion propagator used in ref. [20]. In the present work we refer to it as a "reorientational propagator" (as opposed to the "rotational-diffusion propagator" in ref. [20] because Fig. 1 shows that molecular reorientation of methane is dominated by the free rotation-like motion rather than rotational diffusion. However, the physical meaning of the propagator is completely equivalent to that used in ref. [20] in that it illustrates the evolution of the probability density distribution of the displacement angle α over a certain time range (in this case, from t = 0 to t = 2 ps). The propagator implicitly contains information about all the Legendre polynomial decay curves and therefore provides a convenient snapshot illustration of the reorientational dynamics of the molecules. It is also instrumental in NMR relaxation theory, where it is used for calculating the spectral densities of motion that lead to the NMR spin-relaxation rates. Therefore, we present this propagator as a complement to the plots of the Legendre polynomial decay curves. It can be seen from Fig. 2 that the distribution of α values becomes uniform by ~1 ps, indicating an essentially complete loss of orientational memory by methane molecules by that time.

Fig. 3 illustrates the same propagator as its angular cross sections at different points in time. It also shows that the orientations of the C–H vectors reach a uniform distribution in the angular space (from 0 to π) by the time of ~1 ps. This justified the selection of 2 ps as the length of sub-trajectories used for the analysis of reorientational dynamics of methane molecules (see Methods 3.3).

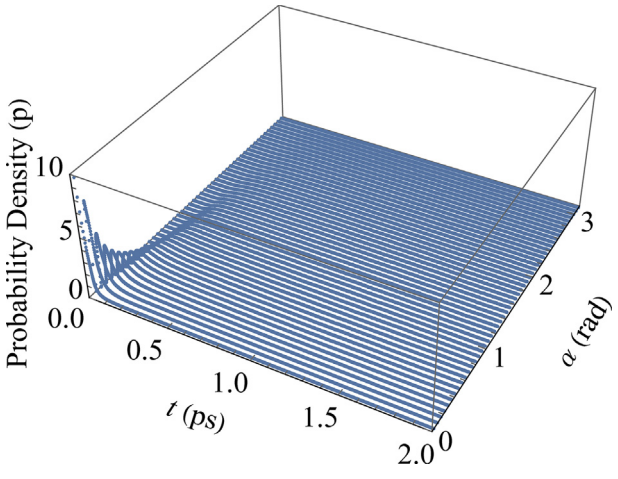

Fig. 2. Three-dimensional view of the uniangular reorientational propagator of methane. The propagator is defined analogously to the uniangular rotational-diffusion propagator used in ref. [20] and shows the loss of molecular "orientational memory" with time (based on the orientation of a single C–H bond). The distribution of angular displacements becomes practically uniform by about 1 ps, indicating a complete loss of orientational memory after ~ 1 ps.

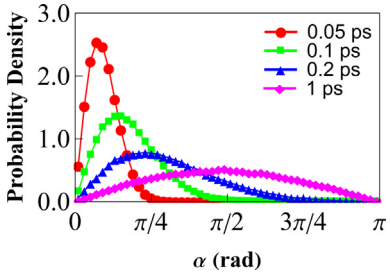

Fig. 3. Angular cross sections of the uniangular reorientational propagator of a C–H vector of methane (Fig. 2) at different times.

Fig. 4 presents the least-squares fits of the Debye model, and the corresponding fit residuals, of a representative temporal slice of the uniangular reorientational propagator. The Figure demonstrates that the full range of the time points (from t = 0 to t = 2 ps) could not be successfully fitted either with the Debye model with a single diffusion coefficient (Eq. (10), the fit shown in Fig. 4a) or with a similar model with two apparent diffusion coefficients (Fig. 4b). With the basic (single-D) Debye model, the fit residuals in the short-time regime exhibited significant systematic deviations (up to 10% of the uniform probability density, see Fig. 4c). No meaningful improvement in the fit residuals was observed when the slice was fitted with a Debye-like model with two diffusion coefficients (see Fig. 4d).

Fig. 5 shows the 3D plot of fit residuals from least-squares fitting of the long-time subset (t = 0.8 ps – 2 ps) of the data points of the 3-dimensional uniangular propagator of liquid methane shown in Fig. 2 with the Debye propagator model, Eq. (10). As seen from Fig. 1, the long-time motion regime is characterised by an exponential decay of the Legendre polynomial correlation functions, and therefore the reorientational propagator in this regime can be expected to follow the Debye model. Indeed, the plot in Fig. 5 shows apparently random residuals. When the temporal range of fitted data was increased to include shorter times, the fit residuals started to exhibit systematic deviations, indicating that the Debye-like behaviour holds only at long times, $t > 0.8$ ps. The value of the rotational diffusion coefficient extracted from least-squares fit used to produce Fig. 5 was (1.911 ± 0.002) ps^{-1}.

5. Discussion

5.1. Molecular mechanics force field

In MD simulations, the accuracy of the simulated macroscopic properties critically depends on the suitability of the force field for the given simulation. This is especially true for simulations of molecular liquids. In MD simulations of liquid water, there is no "universal" water model capable of reproducing all properties of water equally well, and the choice of the force field should therefore be made based on the properties expected to be calculated from the MD simulation [39,40]. This also holds for simulation of hydrated biopolymers [41–43]. Different force fields, which include single-site [31,44,45], multiple-site [46] and all-atom [31–34,47] models, have also been developed and used to simulate methane.

The present study was limited to all-atom force fields of methane. We aimed to identify force fields yielding accurate results for liquid-phase simulations, particularly with respect to reorientational molecular motion. Three all-atom force fields previously used to simulate different properties of methane in the liquid phase were considered. OPLS-compatible parameter set I [31] has been used to successfully reproduce the pressure - density relationship and several transport properties (including translational diffusion coefficient) of methane under a wide range of conditions. Parameter set II [32] has been used to reproduce the radial distribution function, translational

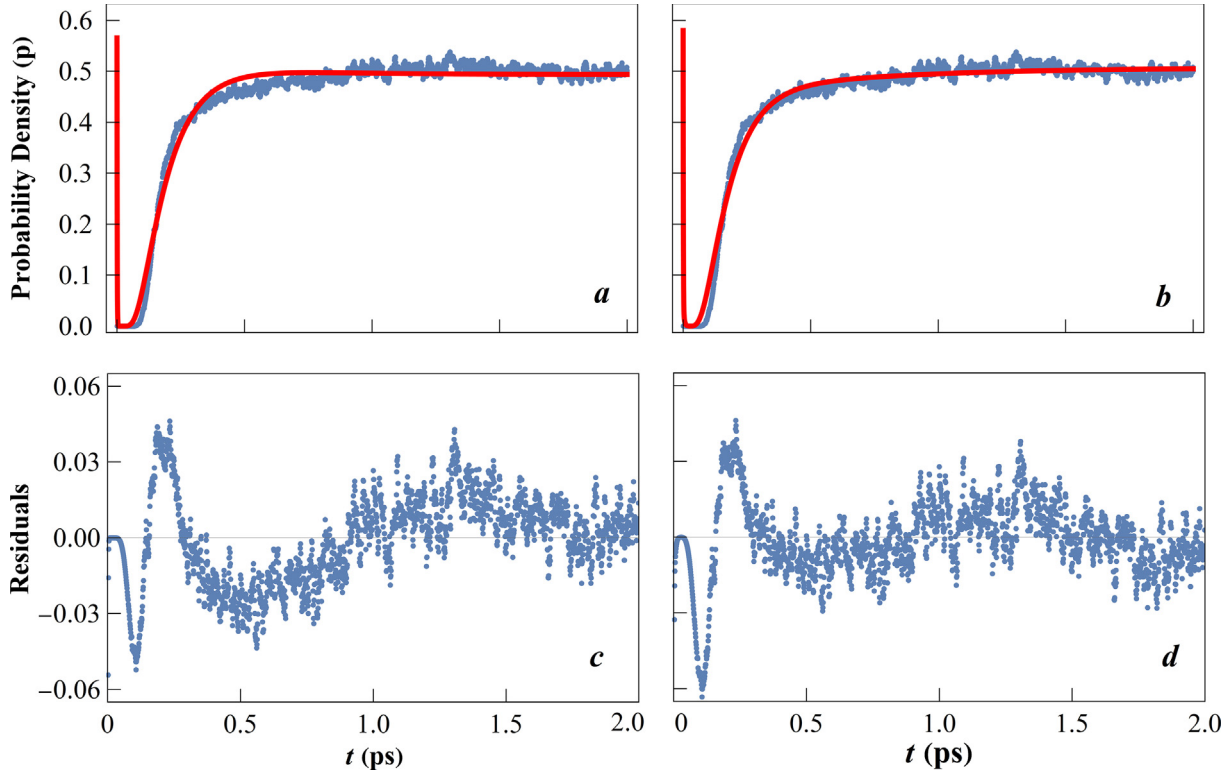

Fig. 4. (a) Representative temporal slice of the MD-simulated uniangular reorientational propagator of methane. The slice represents the range of α from 1.51 rad to 1.57 rad; the time range is the duration of each sub-trajectory described in Methods. The blue dots are the simulated data points; the solid red line is Eq. (10) least-squares fitted with α = 1.54 rad (the basic Debye model with a single D value); (b) the same slice least-squares fitted with the Debye-like model with two diffusion coefficients; (c) the fit residuals corresponding to Fig. 4 (a); and (d) the fit residuals corresponding to Fig. 4(b).

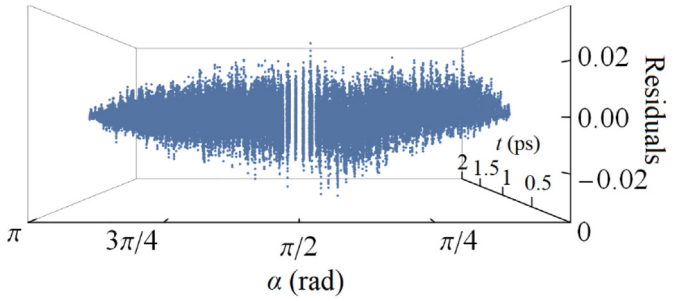

Fig. 5. Plot of the fit residuals obtained from least-squares fitting of the long-time part (t = 0.8–2 ps) of the uniangular reorientational propagator of the C–H vectors of methane with the Debye rotational diffusion propagator model, Eq. (10). The lack of systematic features in the distribution of the residuals demonstrates the Debye-like nature of the reorientational molecular motion at long times. This is consistent with the Legendre polynomial correlation functions shown in Fig. 1.

diffusion coefficient and velocity autocorrelation function of liquid methane using an OPLS energy function. CHARMM-compatible parameter set III [33,34] has been optimised to reproduce the free energies of hydration of amino acid sidechains and the corresponding free molecules. In the present study, we found that parameter set III showed the best performance of the three force fields investigated. We attribute this to the CHARMM energy function being used to calculate the interaction energies in that force field, and specifically to two factors discussed in the following.

Rotational correlation functions of molecules in liquids can be directly derived from the vibrational spectra of the liquid. Therefore, when modelling rotational dynamics of molecules in a liquid, it is important to have an accurate representation of molecular vibrations in the molecular mechanics force field used for the simulation. In methane, the relevant molecular vibrations include the C–H bond vibrations and the angle-bending term of the potential energy function. For the latter, the CHARMM potential function (including parameter set III) includes a correction known as the Urey-Bradley term, which accounts for the non-bonded interactions between atoms 1 and 3 of the bond angle 1–2-3 [30]. Although frequently neglected as small, the Urey-Bradley correction can be used to refine the frequencies of the bond-angle modes in the vibrational spectra of molecules. Its importance is emphasised in literature for tetrahedral systems, including methane [48–51]. Parameter set III in this study outperformed the other two sets of parameters in reproducing the experimental values of density, radial distribution function, and the rotational correlation functions of methane. We hypothesise that part of the reason for this is the inclusion of the Urey-Bradley term in parameter set III.

It should also be noted that parameter sets I and II have been optimised to be used with the OPLS force field. Transferring parameters optimised for one force field to a different force field does not guarantee a performance similar to the original, which may also explain the failure of parameter sets I and II in the present study. Parameter set III has been originally optimised to be used with the CHARMM force field, and therefore had an apparent *a priori* advantage over the other two force fields. We attribute the superior performance of parameter set III to the presence of the Urey-Bradley correction term and the fact that this set was developed specifically as a CHARMM parameter set.

5.2. Reorientational molecular motion in liquids: General considerations

The hallmark of molecular rotational diffusion in liquids is the exponential decay of ensemble-averaged reorientational Legendre polynomial functions. Conversely, free-rotation regime is characterised by the Gaussian decay of the reorientational Legendre polynomials. In the present study, we observed both these regimes: exponential decay of

the reorientational Legendre correlation functions in the long-time regime and Gaussian decay in the short-time regime. We have analysed these two regimes separately. This simplifies the mathematical expressions involved in the analysis, while providing a good approximation of the rotational behaviour of methane molecules in the liquid. The main focus of the present study was to compare the mechanisms underpinning molecular reorientation of spherically symmetric, non-hydrogen bonding molecules in liquids with those seen in hydrogen-bonding liquids.

The present analysis was based on the dynamics of a single intramolecular C–H vector in a given methane molecule. As methane is a spherical top with the T_d symmetry, we do not expect the findings of an analysis based on an intramolecular H–H vector to materially differ from our results. However, a direct confirmation of this in a future investigation may be beneficial.

5.3. Reorientation of liquid methane in the short-time regime

The ensemble-averaged reorientational Legendre polynomial functions of liquid methane exhibited a Gaussian, rather than exponential, behaviour in the short-time regime ($t < 0.2$ ps). This is consistent with experimental data: dipole correlation functions calculated from infrared and Raman spectroscopic data [1,4,29,52] and neutron scattering data [6] have revealed the non-Debye nature of the rotational dynamics of molecules in simple liquids. When the intramolecular component of the longitudinal spin relaxation rate constant was calculated by assuming the values of rotational diffusion coefficients given by the Stokes-Einstein relationship, poor agreement with the experimental values was observed [5]. The non-applicability of the Debye rotational-diffusion model to the rotational dynamics of methane has been attributed to the Debye model's inherent assumption of the rotational correlation time being much longer than the angular momentum correlation time. Under these conditions the angular momentum of a molecule resets many times during the time it takes the molecule to reorient through an angle ~π/2, leading to an "overdamped" rotational-diffusion process. This assumption does not hold for liquid methane, where the rotational correlation time and angular momentum correlation time are comparable [24]. Furthermore, Debye model assumes that the rotation of a molecule occurs through small diffusive angular steps, while infrared and Raman spectroscopic data suggest that the molecules can reorient through large angles in liquids as well as gases [29].

The free-rotation model is widely used to describe the reorientation of molecules in the gas phase [7,29,53,54]. It has been demonstrated that the free-rotation model is also capable of explaining the rotational dynamics of small molecules in certain liquids [29]. Orientational correlation functions based on the free-rotation model have been found to be in good agreement with the experimentally obtained orientational correlation functions of methane [3,4,6,28]. For spherical-top molecules, if the rotation is equivalent to that of a rigid rotator, the equation of motion is given by a Langevin-like equation with linear velocities replaced by angular velocities [55]. It can be shown that the time dependence of the distribution of the molecular orientational displacements in this case is given by a sum of exponential terms ($\exp[-\xi t/I]$) when $\xi t/I >> 1$ (where ξ is the friction coefficient). Conversely, when $\xi t/I << 1$, it is given by a sum of Gaussians of the type $\exp.[-J(J+1)(kT/2I)t^2]$. In the short-time limit, therefore, the reorientational motion depends only on the kinetic energy and the tensor of inertia of the molecule and is independent of the friction coefficient, thus exhibiting the characteristics of gas-like free rotation [56,57]. Recent MD-based studies have shown that the spin-rotational contribution to the experimentally measured ^{1}H NMR spin-relaxation rates of methane under a wide range of conditions is explained well by this "kinetic model" in the gas phase and by the "diffusion model" in the liquid phase [58]. Diffusion model also explains the properties of larger hydrocarbons confined to nanopores [59].

Our results show that the evolution of the reorientational Legendre-polynomial functions of methane in the short-time regime (0–0.2 ps) can be either modelled by the exact free-rotation model or approximated by a Gaussian function. The former is based on an actual physical interpretation of molecular motion, while the latter is a formal mathematical approximation of the physical model. The apparent Gaussian nature of the short-time Legendre correlation functions therefore suggests that in the short-time limit the reorientation of methane molecules is free rotation-like, in the sense of angular momentum correlation time being comparable to the reorientational correlation time.

5.4. Reorientation of liquid methane in the long-time regime

Examination of Fig. 1(*a*) reveals that in the long-time regime ($t >$ ~0.2 ps) the Legendre polynomial functions exhibit a linear decay in the semilog coordinates, corresponding to an exponential decay of $P_l(t)$. The relative amplitude of the exponential component decreases with the increasing l, and in the case of $l = 3$ and 4 this part of the plot is significantly overwhelmed by artifactual features. For this reason, the least-squares fitting of the exponential regime was performed only for $l = 1$ and 2.

The exponential form of the decay in this regime suggests that the molecular rotation on these time scales is sufficiently hindered to be diffusion-like. This is supported by the finding that, at $t > 0.8$ ps, the reorientational propagator of the methane molecules was consistent with the Debye model with a single rotational-diffusion coefficient. Hindered molecular reorientation driven by stochastic intermolecular forces is the fundamental assumption underpinning Debye's rotational-diffusion model. But interestingly, the ratio of the time constants of the two polynomials τ_2^{-1}/τ_1^{-1} is inconsistent with the Debye model: it is close to 1 rather than the theoretical Debye value of 3. Deviations of the MD-simulated ratio τ_2^{-1}/τ_1^{-1} from the Debye value of 3 have been observed in liquid water, where they were attributed to the presence of discrete large-angle orientational jumps superimposed on rotational diffusion [14,15,20]. However, the value of the ratio τ_2^{-1}/τ_1^{-1} observed in the present study (1.2) is significantly lower than the lowest possible theoretical value of $\tau_2^{-1}/\tau_1^{-1} = 1.8$ provided by Ivanov's jump model [13]. It is also significantly lower than the values observed in MD simulations of liquid water, which were between 1.95 and 2.1 [15,20]. Therefore, the presence of discrete jumps fails to explain the discrepancy between the exponential regime seen in Fig. 1 and the Debye model. Therefore, we refer to this regime as "Debye-like". This nomenclature is meant to point out the exponential nature of the decay $P_l(t)$ and the Debye form of the long-time reorientational propagator, but also to emphasise the deviation from the true Debye model.

At this stage, we are unable to conclusively ascertain the exact nature of the "Debye-like" exponential regime. However, the following observations appear important:

1) The exponential regime is observed not only in the semilog plots (Fig. 1(*a*)) but also in the original coordinates, P_l *vs* t. Therefore, it is not an artifact of the semilog coordinate transformation;
2) The amplitude of the exponential component is significantly greater than statistical noise. It is also greater than the amplitude of the oscillatory artifacts seen in Fig. 1(*a*) and particularly prominent for $l = 3$ and 4;
3) A visual comparison of the slopes of the four plots ($l = 1$–4) suggests that the apparent exponential time constant in this regime is either independent or nearly independent of the value of l.

We believe that these observations provide important clues into the nature of the Debye-like regime. Its origin will be the subject of future research.

5.5. Decay of the Legendre polynomials: whole-curve fitting

Fig. 1(*a*) clearly shows the existence of two regimes in the decay of the reorientational Legendre polynomials: the initial Gaussian decay followed by an exponential decay. However, attempts to fit the

polynomial $P_1(t)$ with a linear combination of a single Gaussian and a single exponential function were unsuccessful: the best fit using this model exhibited strong systematic distortions with non-random residuals of up to 5% amplitude (relative to the value of P_1 at $t = 0$). On the other hand, the model that included a second exponential component (Eq. (9)) yielded an excellent fit with the relative residuals not exceeding 0.3%. The origin of the second apparent exponential component can be intuitively explained in terms of the Wiener-Khinchin theorem. While the following analysis is not absolutely rigorous mathematically, it provides a qualitative justification of the form of Eq. (9).

Consider a stochastic process, $f(t)$, that is a superposition of a free rotation-like process, $s(t)$ (characterised by a Gaussian autocorrelation function and a Gaussian spectral density of motion) and a diffusion-like process, $r(t)$ (characterised by an exponential autocorrelation function and a Lorentzian spectral density of motion):

$$f(t) = s(t) + r(t) \tag{12}$$

The Legendre polynomial $P(t)$ is a self-convolution of the of the stochastic function $f(t)$. Since the Fourier transform of a convolution is the product of the respective Fourier transforms of the functions being convoluted, the Fourier transform of $P(t)$, $P(\omega)$, equals the power of the Fourier transform of $f(t)$, $F(\omega)$:

$$P(\omega) = F^2(\omega) \tag{13}$$

According to Eq. (12), $F(\omega)$ is a linear combination of a complex function whose square is a Lorentzian, and another complex function whose square is a Gaussian. Therefore, the Fourier transform of the Legendre polynomial, $P(\omega)$, is a linear combination of a Lorentzian (Term 1, diffusion-like process), a Gaussian (Term 2, free rotation-like process), and a function whose envelope can be approximated by a product of a Lorentzian and a Gaussian function (Term 3). An inverse Fourier transform of $P(\omega)$ enables the reconstruction of the general form of the original Legendre polynomial temporal function, $P(t)$: Term 1 of $P(\omega)$ leads to an exponential function of time; Term 2 produces a Gaussian function; and the inverse Fourier transform of Term 3 can be approximated as a convolution between an exponential and a Gaussian function, which has an exponential form. This last term can be interpreted as the second exponential term in Eq. (9). Therefore, the presence of the second exponential component in Eq. (9) does not imply the presence of a second Debye-like process in the reorientational dynamics of methane molecules; rather, it represents a cross-correlation between the Gaussian and the Debye-like process.

The Legendre polynomials P_2 - P_4 did not require the second exponential component in the fitting model: a linear combination of a single exponential and a single Gaussian term provided a good whole-curve fit for these polynomials. This can be explained by the small relative amplitude of the Debye-like exponential component in the case of $l = 2$–4, resulting in a negligibly small cross-term.

5.6. The role of intermolecular interactions

Intermolecular interactions play an important role in determining the mechanism and the nature of molecular rotation in liquids. The lack of free-rotation characteristics in the Raman wings of liquids is in general attributed to the hindering of molecular rotation by intermolecular forces [29], and in this case the dissipative component of intermolecular interactions averages to an isotropic viscous drag given by the Stokes-Einstein relationship. Due to dipole moments and hydrogen bonding, the intermolecular interactions are large in liquids such as water and ammonia; therefore, the molecules in these liquids do not exhibit free rotation. In low-molecular weight hydrocarbons, the relatively low boiling temperatures and latent heats of vaporisation are indicators of the relatively small magnitude of intermolecular interactions: indeed, the intermolecular forces between methane molecules are much smaller than those between water molecules in the liquid state [29]. Therefore, we suggest that the effect of intermolecular interactions on the rotational dynamics of methane molecules in liquid methane is relatively small on the short time scales, when the molecular reorientation is described by the free-rotation model. On longer time scales (~0.5 ps and up), the cumulative work performed by intermolecular forces eventually becomes significant, and as the time increases, the molecules gradually reach the overdamped, hindered-rotation limit characterised by the exponential decay of $<P_1>$ and $<P_2>$. The presence of the free-rotation regime explains how methane molecules can achieve a complete loss of orientational memory much faster (~2 ps, see Fig. 3) than water molecules (~100 ps, see Fig. 3 in ref. [20]). Conversely, in liquid water the large-angle jumps are only occasional and superimposed on incremental diffusional steps. In the "hindered" long-time regime, the reorientation of methane molecules was also significantly faster than water: the apparent rotational diffusion coefficient of methane was ~2 ps^{-1} at 98 K, compared to ~0.1 ps^{-1} at 298 K for water. This can also be attributed to the relatively low intermolecular interactions between methane molecules (including the absence of hydrogen bonds), which in turn results in a significantly lower viscosity than that of water.

6. Conclusions

Although methane is a spherically symmetric, non-hydrogen-bonding molecule, the traditional Debye model fails to describe the rotational dynamics of methane molecules in liquid methane. In the long-time regime, methane molecules do exhibit Debye-like behaviour characterised by an exponential decay of the reorientational Legendre polynomials and the rotational-diffusion propagator with a single diffusion coefficient. The latter feature is in contrast to the rotational dynamics of liquid water, where two apparent rotational-diffusion coefficients were needed to empirically approximate the rotational-diffusion propagator of water molecules. We attribute this difference to the strong hydrogen-bonding network of liquid water, which is lacking in methane. As expected from the relatively small magnitude of intermolecular interactions in liquid methane, the rotational diffusion coefficient of methane was found to be considerably larger than that of water, corresponding to a much shorter time of orientational randomisation compared to water.

Unexpectedly, the ratios of the Legendre polynomial time constants in the long-time regime were inconsistent with the Debye model's ideal values (1 : 3 : 6 : 10) and, in fact, exhibited no clear dependence on the order of the Legendre polynomial. This finding requires further investigation.

In the short-time regime (<0.2 ps) the rotational dynamics of liquid methane failed to obey the Debye model entirely. In this regime the reorientational Legendre polynomials exhibited a Gaussian decay, corresponding to the gas-like free-rotation model rather than rotational diffusion.

These results call for further development of NMR spin-relaxation theory, where molecular reorientation is usually the principal factor controlling the relaxation of nuclear magnetisation.

Declaration of Competing Interest

The authors declare that they have no known competing financial interests or personal relationships that could have appeared to influence the work reported in this paper.

Acknowledgements

Supercomputing resources and services used in this work were provided by the High Performance Computing Centre and Research Support Group (HPC), Queensland University of Technology, and by the

Department of Physics, University of Colombo. This work was financially supported by the University of Colombo, Postgraduate Research Grant AP/3/ 2/2015/PG/08.

Appendix A. Supplementary data

Supplementary data to this article can be found online at https://doi.org/10.1016/j.molliq.2020.114727.

References

[1] R.G. Gordon, Molecular motion in infrared and Raman spectra, J. Chem. Phys. 43 (1965) 1307–1312.
[2] R.G. Gordon, Relations between Raman spectroscopy and nuclear spin relaxation, J. Chem. Phys. 42 (1965) 3658–3665.
[3] H. Shimizu, Time-correlation function of molecular random motion and shape of spectral bands, J. Chem. Phys. 43 (1965) 2453–2465.
[4] A. Cabana, R. Bardoux, A. Chamberland, Infrared spectra, rotational correlation functions, band moments and intermolecular mean squared torques of methane dissolved in liquid Noble gases, Can. J. Chem. 47 (1969) 2915–2920.
[5] J.H. Rugheimer, P.S. Hubbard, Nuclear Magnetic Relaxation and Diffusion in Liquid CH4, CF4, and Mixtures of CH4 and CF4 with Argon, J. Chem. Phys. 39 (1963) 552–564.
[6] V.F. Sears, Cold neutron scattering by molecular liquids: III. Methane, Can. J. Phys. 45 (1967) 237–254.
[7] V.F. Sears, Theory of cold neutron scattering by homonuclear diatomic liquids i. free rotation, Can. J. Phys. 44 (1966) 1279–1297.
[8] V.F. Sears, Theory of cold neutron scattering by homonuclear diatomic liquids II. Hindered Rotation, Can. J. Phys. 44 (1966) 1299–1311.
[9] J. Teixeira, A. Luzar, S. Longeville, Dynamics of hydrogen bonds: how to probe their role in the unusual properties of liquid water, J. Phys. Condens. Matter 18 (2006) 2353–2362.
[10] P. Debye, Polar Molecules, Dover Publications, New York, 1928.
[11] A. Abragam, The Principles of Nuclear Magnetism, Clarendon Press, Oxford, 1962.
[12] F. Perrin, Brownian motion of an ellipsoid I. dielectric dispersion for ellipsoidal molecules, J. Phys. Radium. 5 (1934) 497–511.
[13] E.N. Ivanov, Theory of rotational Brownian motion, Sov. Phys. J. 18 (1964) 1041–1045.
[14] D. Laage, J.T. Hynes, A molecular jump mechanism of water reorientation, Science 311 (2006) 832–835.
[15] D. Laage, J.T. Hynes, On the molecular mechanism of water reorientation, J. Phys. Chem. B 112 (2008) 14230–14242.
[16] D. Laage, Reinterpretation of the liquid water quasi-elastic neutron scattering spectra based on a nondiffusive jump reorientation mechanism, J. Phys. Chem. B Lett. 113 (2009) 2684–2687.
[17] D. Laage, G. Stirnemann, F. Sterpone, R. Rey, J.T. Hynes, Reorientation and allied dynamics in water and aqueous solutions, Annu. Rev. Phys. Chem. 62 (2011) 395–416.
[18] R. Ludwig, The mechanism of the molecular reorientation in water, ChemPhysChem. 8 (2007) 44–46.
[19] C. Calero, J. Martí, E. Guàrdia, 1 H nuclear spin relaxation of liquid water from molecular dynamics simulations, J. Phys. Chem. B 119 (2015) 1966–1973.
[20] W.A.M. Madhavi, S. Weerasinghe, K.I. Momot, Rotational-diffusion propagator of the intramolecular proton–proton vector in liquid water: a molecular dynamics study, J. Phys. Chem. B 121 (2017) 10893–10905.
[21] A. Luzar, D. Chandler, Hydrogen-bond kinetics in liquid water, Nature. 379 (1996) 55–57.
[22] M. Shafiei, M. Von Domaros, D. Bratko, A. Luzar, Anisotropic structure and dynamics of water under static electric fields, J. Chem. Phys. 150 (2019) 074505 .
[23] R.G. Gordon, On the rotational diffusion of molecules, J. Chem. Phys. 44 (1966) 1830–1836.
[24] R.E.D. McClung, Rotational diffusion of spherical-top molecules in liquids, J. Chem. Phys. 51 (1969) 3842–3852.
[25] W.A.M. Madhavi, S. Weerasinghe, K.I. Momot, Effects of hydrogen bonding on the rotational dynamics of water-like molecules in liquids: insights from molecular dynamics simulations, Aust. J. Chem. 73 (2020) 734–742.
[26] S. Schaack, U. Ranieri, P. Depondt, R. Gaal, W.F. Kuhs, A. Falenty, P. Gillet, F. Finocchi, L.E. Bove, Orientational ordering, locking-in, and distortion of CH4 molecules in methane hydrate III under high pressure, J. Phys. Chem. C 122 (2018) 11159–11166.
[27] S. Schaack, U. Ranieri, P. Depondt, R. Gaal, W.F. Kuhs, P. Gillet, F. Finocchi, L.E. Bove, Observation of methane filled hexagonal ice stable up to 150 GPa, Proc. Natl. Acad. Sci. U. S. A. 116 (2019) 16204–16209.
[28] R.E.D. McClung, T.E. Eagles, Rotational diffusion of spherical top molecules in liquids. III. Semiclassical rotational diffusion model and the infrared band shapes of CH4 in Gaseous and liquid mixtures, J. Chem. Phys. 59 (1973) 435–444.
[29] M.F. Crawford, H.L. Welsh, J.H. Harrold, Rotational wings of Raman bands and free rotation in liquid oxygen, nitrogen and methane, Can. J. Phys. 30 (1952) 81–98.
[30] A.D. MacKerell, D. Bashford, M. Bellott, R.L. Dunbrack, J.D. Evanseck, M.J. Field, S. Fischer, J. Gao, H. Guo, S. Ha, D. Joseph-McCarthy, L. Kuchnir, K. Kuczera, F.T.K. Lau, C. Mattos, S. Michnick, T. Ngo, D.T. Nguyen, B. Prodhom, W.E. Reiher, B. Roux, M. Schlenkrich, J.C. Smith, R. Stote, J. Straub, M. Watanabe, J. Wiórkiewicz-Kuczera, D. Yin, M. Karplus, All-atom empirical potential for molecular modeling and dynamics studies of proteins †, J. Phys. Chem. B 102 (1998) 3586–3616.
[31] C.G. Aimoli, E.J. Maginn, C.R.A. Abreu, Transport properties of carbon dioxide and methane from molecular dynamics simulations, J. Chem. Phys. 141 (2014) 134101.
[32] C. Jiang, J. Ouyang, X. Zhuang, L. Wang, W. Li, An efficient fully-atomistic potential model for dense fluid methane, J. Mol. Struct. 1117 (2016) 192–200.
[33] F. Pietra, On Dioxygen and substrate access to soluble methane Monooxygenases: an all-atom molecular dynamics investigation in water solution, Chem. Biodivers. 14 (2017) e1600158 .
[34] M.R. Shirts, J.W. Pitera, W.C. Swope, V.S. Pande, Extremely precise free energy calculations of amino acid side chain analogs: comparison of common molecular mechanics force fields for proteins, J. Chem. Phys. 119 (2003) 5740–5761.
[35] W.L. Jorgensen, D.S. Maxwell, J. Tirado-Rives, Development and testing of the OPLS all-atom force Field on conformational energetics and properties of organic liquids, J. Am. Chem. Soc. 118 (1996) 11225–11236.
[36] U. Setzmann, W. Wagner, A new equation of state and tables of thermodynamic properties for methane covering the range from the melting line to 625 K at pressures up to 100 MPa, J. Phys. Chem. Chem. Ref. Data. 20 (1991) 1061–1155.
[37] A. Habenschuss, E. Johnson, A.H. Narten, X-ray diffraction study and models of liquid methane at 92 K, J. Chem. Phys. 74 (1981) 5234–5241.
[38] B.G. Levine, J.E. Stone, A. Kohlmeyer, Fast analysis of molecular dynamics trajectories with graphics processing units-radial distribution function Histogramming, J. Comput. Phys. 230 (2011) 3556–3569.
[39] C. Vega, J.L.F. Abascal, Simulating water with rigid non-polarizable models: a general perspective, Phys. Chem. Chem. Phys. 13 (2011) 19663–19688.
[40] P. Mark, L. Nilsson, Structure and dynamics of the TIP3P, SPC, and SPC/E water models at 298 K, J. Phys. Chem. A 105 (2001) 9954–9960.
[41] M.R. Shirts, V.S. Pande, Solvation free energies of amino acid side chain analogs for common molecular mechanics water models, J. Chem. Phys. 122 (2005).
[42] M.C. Tourell, K.I. Momot, Molecular dynamics of a hydrated collagen peptide: insights into rotational motion and residence times of single-water bridges in collagen, J. Phys. Chem. B 120 (2016) 12432–12443.
[43] W.A.M. Madhavi, S. Weerasinghe, G.D. Fullerton, K.I. Momot, Structure and dynamics of collagen hydration water from molecular dynamics simulations: implications of temperature and pressure, J. Phys. Chem. B 123 (2019) 4901–4914.
[44] F. Betaouaf, F. Cailliez, B. Rousseau, F. Ould-Kaddour, Molecular simulation of the thermodynamics, structural and transport properties of the liquid binary mixture methane + nitrogen, J. Mol. Liq. 200 (2014) 298–304.
[45] A. Kadoura, A.K. Narayanan Nair, S. Sun, Molecular dynamics simulations of carbon dioxide, methane, and their mixture in Montmorillonite clay hydrates, J. Phys. Chem. C 120 (2016) 12517–12529.
[46] S.-W. Chao, A.H. Li, S.D. Chao, Molecular dynamics simulations of fluid methane properties using Ab initio intermolecular interaction potentials, J. Comput. Chem. 30 (2010) 1839–1849.
[47] M. Oobatake, S. Hayashi, K. Machida, Molecular dynamics simulation of structure of liquid methane, Bull. Inst. Chem. Res. Kyoto Univ. 68 (1990) 255–264.
[48] J.P. Devlin, Urey-Bradley "Nonbonded" forces, J. Chem. Phys. 39 (1963) 2385–2385.
[49] E.J. Slowinski, New form of molecular potential function for use in molecular vibrational analysis, J. Chem. Phys. 23 (1955) 1933–1935.
[50] N.D. Heitkamp, Hindered internal rotation and the Urey-Bradley force field: Part I. Consideration of Non-Bonded Interaction in a Five-Atom Configuration, J. Mol. Spectrosc. 19 (1966) 332–338.
[51] H.C. Urey, J. Charles, A. Bradley, The vibrations of pentatonic tetrahedral molecules, Phys. Rev. 38 (1931) 1969–1978.
[52] G.E. Ewing, Spectroscopic studies of molecular motion in liquids, Acc. Chem. Res. 2 (1969) 168–174.
[53] T.E. Eagles, R.E.D. Mcclung, Rotational diffusion of spherical top molecules in liquids and Gases. IV. Semiclassical Theory and Applications to the V3 and Band Shapes of Methane in High Pressure Gas Mixtures, J. Chem. Phys. 61 (1974) 4070–4082.
[54] A.G.St. Pierre, W.A. Steele, Collisional effects upon rotational correlations of symmetric top molecules, J. Chem. Phys. 57 (1972) 4638–4648.
[55] W.A. Steele, Molecular Reorientation in Liquids. I. Distribution Functions and Friction Constants, J. Chem. Phys. 38 (1963) 2404–2410.
[56] W.A. Steele, Molecular Reorientation in Liquids. II. Angular Autocorrelation Functions, J. Chem. Phys. 38 (1963) 2411–2418.
[57] P.M. Singer, D. Asthagiri, Z. Chen, A.V. Parambathu, G.J. Hirasaki, W.G. Chapman, Role of internal motions and molecular geometry on the NMR relaxation of hydrocarbons, J. Chem. Phys. 148 (2018) 164507.
[58] P.M. Singer, D. Asthagiri, W.G. Chapman, G.J. Hirasaki, NMR spin-rotation relaxation and diffusion of methane, J. Chem. Phys. 148 (2018) 204504.
[59] A. Valiya Parambathu, P.M. Singer, G.J. Hirasaki, W.G. Chapman, D. Asthagiri, Critical role of confinement in the NMR surface relaxation and diffusion of n-heptane in a polymer matrix revealed by MD simulations, J. Phys. Chem. B 124 (2020) 3801–3810.